International Journal of Scientific Engineering and Research (IJSER)
ISSN (Online): 2347-3878
Impact Factor (2020): 6.733

Synthesis and Characterisation of $Na_2Ba_{1-x}Eu_xMg$ $(PO_4)_2$

C Shankaraiah, V. Gangadhar, G. Prasad, M. Srinivas*

Department of Physics, Osmania University, Hyderabad 500 007, India

Abstract: ***The Na2Ba1-xEuxMg (PO4) 2 (x=0, 1%, 3% and 5%) compound was prepared by high temperature solid state reaction method. The X-ray crystallographic studies were carried out using diffraction at 30°C in two theta range of 10-80°. The crystal structure of the sample is rhombohedral and the space group is P-3m1. The pure Na2BaMg (PO4) 2 doped with Europium form samples with good density and well defined morphology. Increase in doping leads to decreasing the grain size. FT-IR spectra of the samples are studied in the wavelength region of 250-4000 cm-1. Impedance and dielectric measurements are undertaken. Photoluminescence europium doped samples are studied.***

Keywords: Impedance, dielectric, FTIR, Photoluminescence

1. Introduction

The Phosphate compounds are multifunctional materials [1]. These materials have ability to convert voltage into light and their functionality as light emitting diodes are exploited to an advantage. They have high quantum efficiency, long life time, high energy efficiency, high stability and are eco-friendly [2]. Rare earth doped phosphate compounds have also became important due to their possible application for sensors and batteries [3]. Phosphate compounds are used as phosphors in fluorescent lamps for their low cost, easy synthesis methods and high chemical stability [4, 5].

In Na2BaMg (PO4) 2 compounds doped with Ce^{+3}, Mn^{+2} doping ions can change the color tone of emitted radiation gradually with the control of Mn content and finally reach red region [4]. Na_2BaMg (PO4) 2: Sr material was studied for the photoluminescence with the europium doping showed that the trivalent europium can replace for both the strontium and magnesium. The effect of europium on the blue emission is reported. [5, 6]. Among doped Na2BaMg (PO4) 2 based compounds, Mn^{+2} doped compound showed a weak red emission by low wave length excitation. Ce^{3+} doped sample showed strong near –UV radiation with UV light. Eu^{2+}or Ce^{3+} co-doping has resulted in resonance effects from Eu^{2+} or Ce^{3+} to Mn^{2+} [7], Luminescence properties are investigated with blue light excitation, which can be sued in LED Chips [8], Na2BaMg (PO4) 2: Tb^{+3}, Eu^{+2} samples show blue and green emissions [8-10].

Eu^{+3} ion has a transactions from $^5D_0$ level and next lower $^7F_6$ level [12, 13] and will give red line. In this present work Eu+3 ions are doped into Na_2BaMg $(PO_4)_2$. These sodium phosphate materials are synthesized by solid state method. Compound synthesized has composition $Na_2Ba_{1-x}Eu$ (PO_4) $_2$ with X=0 (NMBMP), 1% (NMBMP1), 3% (NMBMP3), 5% (NMBMP5)). The samples are characterized by X-ray diffraction (XRD), Scanning electron microscopy (SEM), Energy dispersion spectroscopy (EDS). The Fourier Transform Infrared spectroscopy (FTIR), dielectric spectroscopy and luminescence emission studies are undertaken.

2. Experimental

The $Na_2Ba_{1-x}Eu_xMg$ $(PO_4)_2$ (where x= x=0, 1%, 3% and 5%-abbreviated as NBMP, NBMP1, NBMP3 and NBMP5 respectively) were prepared using high temperature solid state method. The raw materials Na_2CO_3, Ba_2O_3, MgO, $NH_4H_2PO_4$, and Eu_2O_3 were weighed in Stoichiometric ratio. The powders were mixed uniformly and ground thoroughly using mortor and pestle and ethanol solvent was used during grinding for ensuring the homogeneous mixing of powders. The mixtures were taken in ceramic crucibles and calcined at temperature 800° C for 3 hours. The samples were heated at 5^0C/Min temperature rate. Calcined powder was compacted (applied pressure of 4.9MPa) into circular disks of 10mm diameter and 2mm thickness, with polyvinyl alcohol (PVA) binder. The circular disk were sintered for 3 hours at 850oC depending on samples.

XRD studies of the samples were carried out by with Rigaku-Miniflex-600 instrument with CuKα radiation with speed of 2° / min from 10° to 80°. The densities of the sintered samples were measured using first principles (Archimedes). The weight in air and weight in Xylene (density of xylene = 0.87. gr/cm3) are used. FTIR Spectra of the samples were recorded at room temperature using a ‘‘BRUKER OPTICS-Model TENSOR-27” in spectral range of 7500-370 cm-1. The morphological studies of the samples were studied using “Carl Zeiss EVO 18 Scanning Electronic Microscope” (SEM). The EDS spectra were recorded with “Oxford EDAX system”. The impedance and dielectric studies are undertaken on circular pellets of the samples using AUTOLAB PG STAT 30 low frequency impedance analyzer. In 100 Hz – 1 MHz and 30 to 500°C range. The circular disks are painted with silver paste to serve as electrodes. The corrected excitation and emission spectra of samples scanned with Shimadzu – RF 6000 Spectro fluorimeter.

3. Results and Discussion

The XRD of $Na_2Ba_{1-x}Eu_xMg$ (PO_4) $_2$ (x= 0, 1%, 3%, and 5%) are shown in Figure 1 (a). These results are compared with ICSD card number # 42 4073 and matched well. Structure of samples is rhombohedral, with space group:

p-3m1, Lattice parameter of the samples calculated by using POWD software and observed a=5.3040Å, c=6.9860Å for NBMP samples [9]. Increasing the concentration of Eu3+ resulted in maximum intensity peak shift to higher 2θ values as shown in Fib.1 (b). This is because the ionic radius of Eu3+ 0.97Å than that of Ba2+ is 1.38Å and smaller Eu3+ should lead to a decrease in the unit cell volume indicating that Eu3+ ions were successfully doped in the Ba site in $Na_2BaMg\ (PO_4)_2$ lattice structure [14-15].

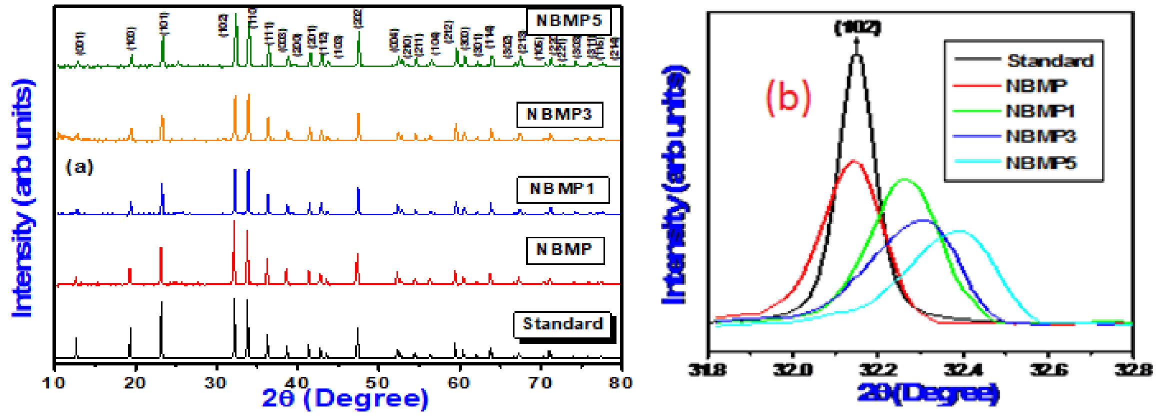

Figure 1 (a): XRD of the NBMP, NBMP1, NBMP3 and NBMP5, **(b)** shifting of peaks to right side

Table 1 also Shows Density of $Na_2Ba_{1-x}Eu_xMg\ (PO_4)_2$ (X=0, 1%, 3%, 5%) samples. From the table 1it can be concluded that the all the samples have high relative density of more than 90%. This means less porosity. This is also confirmed from SEM images. Density of NBMP is less than NBMP1due the increasing the doping concentration of Eu density also increasing except NBMP3. Figure 2 shows the microstructure of the samples recorded at magnification 25kX at 10kV. All grains are in spherical shape. The doping concentration of Eu increases the grain size is decreasing. These results are summarized in Table 2.

Table 1: Structural parameters of NBMP, NBMP1, NBMP3 and NBMP5 samples

Samples Nemonic and x value	a Å	b Å	c Å	c/a Å	Volume $Å^3$	Experimental Density	Theoretical Density	Relative Density (%)
NBMP	5.304	5.304	6.986	1.317	170.203	4.136	3.878	92
NBMP1	5.299	5.299	6.984	1.317	169.911	4.233	3.874	95
NBMP3	5.296	5.296	6.984	1.318	169.696	4.139	3.858	93
NBMP5	5.285	5.285	6.969	1.318	168.582	4.231	3.862	95

Table 2: Grain size of NBMP, NBMP1, NBMP3 and NBMP5 samples

Samples	Grain size (µm)	Crystallite size (nm)
NBMP	2.47	81.66
NBMP1	3.48	44.07
NBMP3	0.95	37.03
NBMP5	0.82	37.58

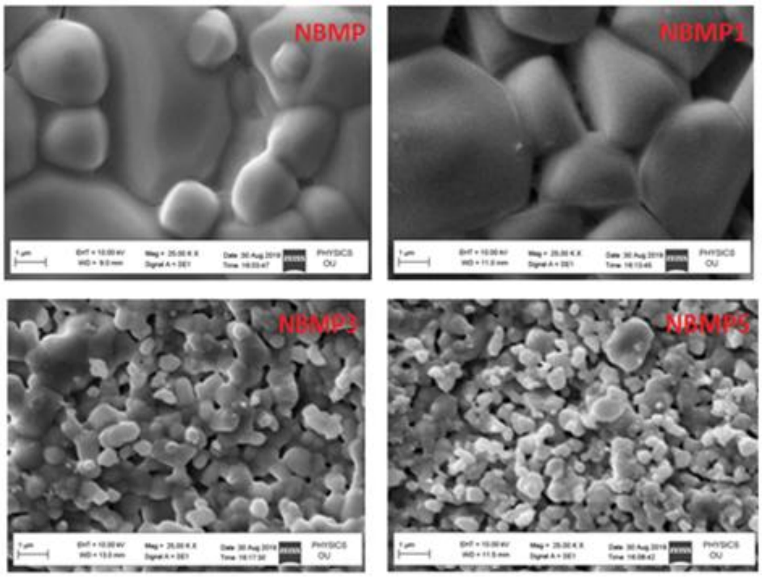

Figure 2: Show SEM images of NBMP, NBMP1, NBMP3 and NBMP5 samples

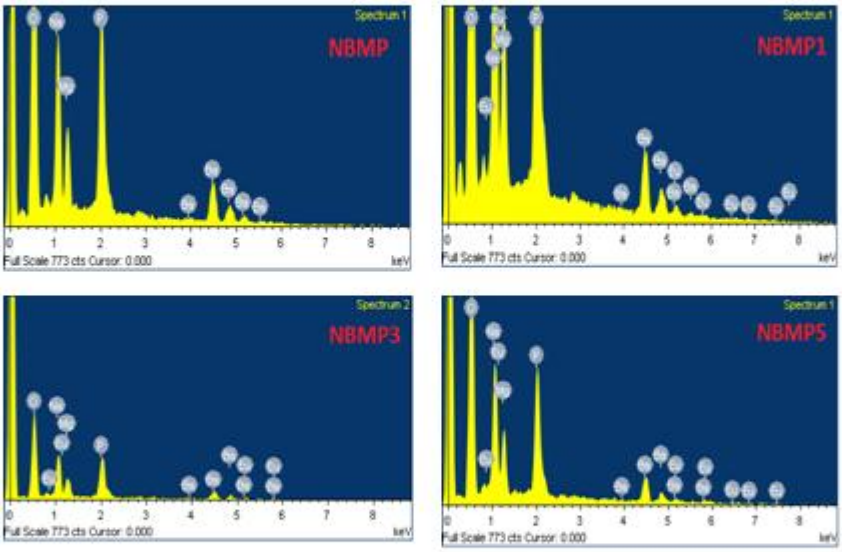

Figure 3: Shows energy dispersive spectra (EDS) of NBMP, NBMP1, NBMP3 and NBMP5 samples

Table 3: EDS data of the NBMP, NBMP1, NBMP3, and NBMP5

			Elements					
			Na	Ba	Eu	Mg	P	O
NBMP	Theoretical	Atomic%	11.57	34.54	-	6.11	15.58	32.19
		Weight%	14.29	7.14	-	7.14	14.29	57.14
	Experimental	Atomic%	10.48	37.48	-	5.11	15.40	31.54
		Weight%	13.38	8.01	-	6.16	14.59	57.86
NBMP1	Theoretical	Atomic%	11.60	33.60	0.77	6.13	15.62	32.28
		Weight%	14.28	6.92	0.14	7.14	14.28	57.14
	Experimental	Atomic%	11.68	30.51	1.62	5.58	15.64	34.98
		Weight%	13.79	6.07	0.29	6.27	13.79	59.71
NBMP3	Theoretical	Atomic%	11.66	31.69	2.31	6.16	15.71	32.46
		Weight%	14.28	6.50	0.43	7.14	14.28	57.14
	Experimental	Atomic%	12.09	33.72	0.82	5.28	15.52	32.56
		Weight%	14.90	6.95	0.15	6.15	14.19	57.65
MBMP5	Theoretical	Atomic%	11.73	29.77	3.88	6.19	15.80	32.64
		Weight%	14.28	6.07	0.72	7.14	14.28	57.14
	Experimental	Atomic%	10.43	32.84	6.20	5.51	13.93	31.09
		Weight%	13.53	7.13	1.22	6.75	13.41	57.96

The EDS spectra of NBMP, NBMP1, NBMP3, and NBMP5 samples shows the presence of Na, Ba, Eu, Mg, P, and O in the desired proportion in the sample. Table 3 shows that the theoretical and experimental atomic and weight percentages in of all elements present in NBMP, NBMP1, NBMP3 and NBMP5. From EDS spectra and table 3 it is concluded that in all the samples the elements are present in desired proportion. Absence of additional peaks shows that impurities are absent in the sample.

Transmission versus wave number of FT-IR of NBMP, NBMP1, NBMP3 and NBMP5 in the wave number region of 250-4000 cm^{-1} ia shown in the figure 4. The peaks at 327, 582, 738, 1035 and 1084 cm^{-1} are due to of stretching of P-O-P bonds (symmetric and asymmetric), while P-O-P bending vibrations are observed in the range of 250-600 cm^{-1}. The absorption in 3000-3700 cm^{-1} is due to stretching vibration of OH, which belongs to absorbed water on the surface of sample from air [4, 16]. In NBMP5 samples the characteristic peaks of PO_3^{-4} ion are seen in the range at 940–1120 cm^{-1} and at 560–650 cm^{-1} [17].

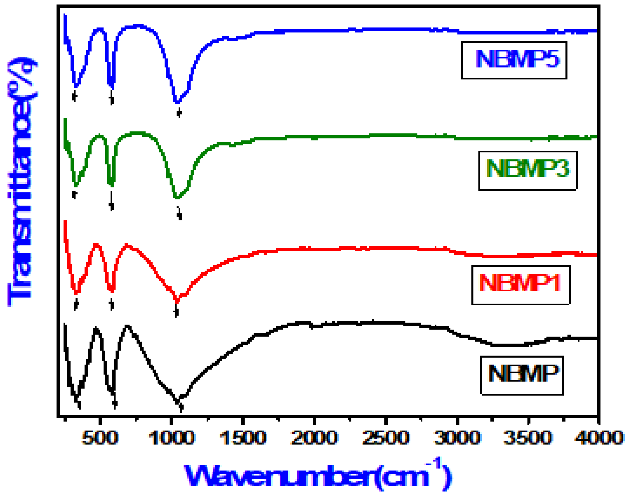

Figure 4: FTIR spectrum of NBMP, NBMP1, NBMP3 and NBMP5 samples

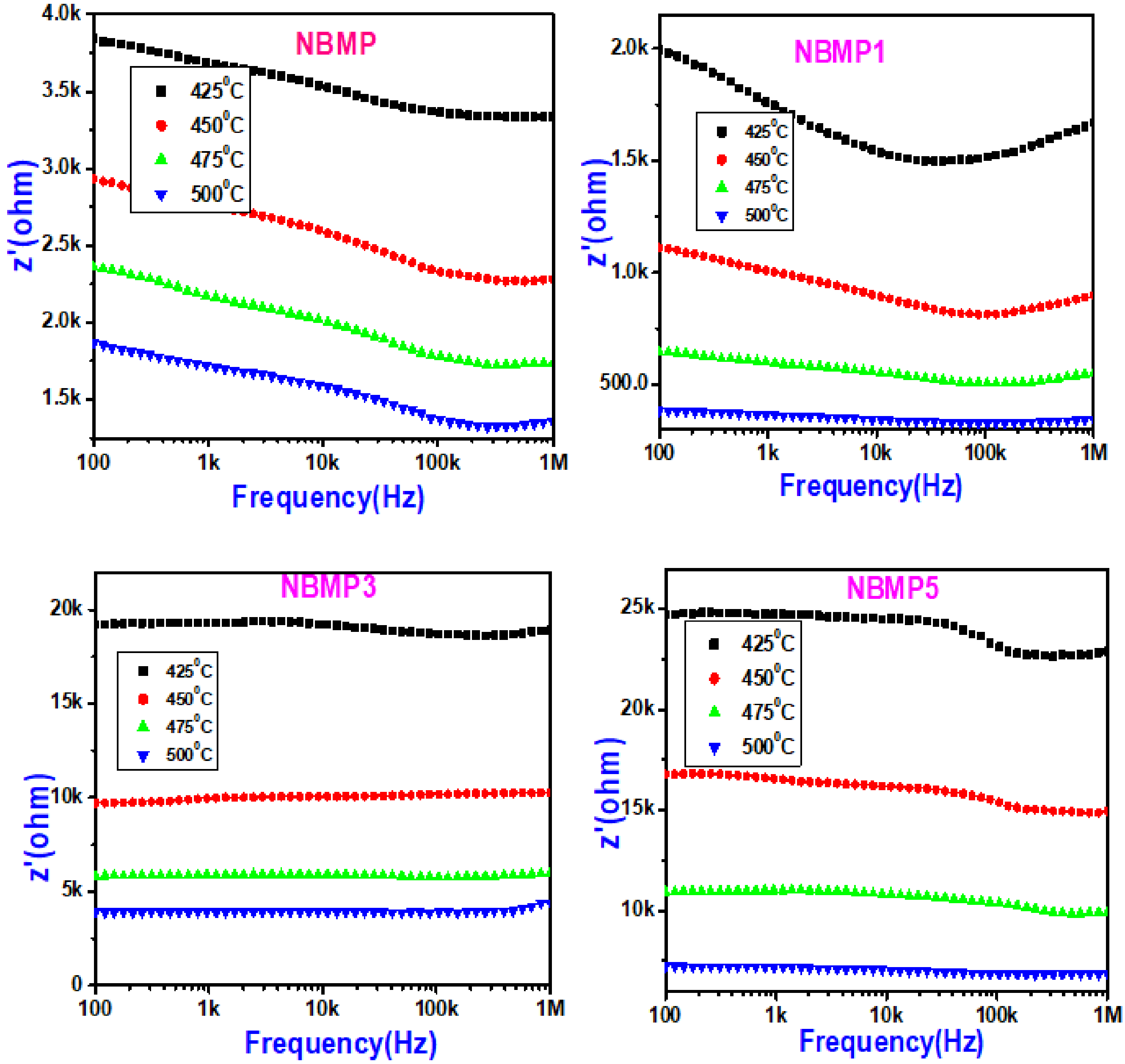

Figure 5: Z' versus frequency of the NBMP, NBMP1, NBMP3 and NBMP5 samples

Figure 5 represent the variation of real part of impedance Z' with frequency for $Na_2Ba_{1-x}Eu_xMg(P_2O_8)$ samples with different compositions. For these samples, the Z' is decreases monotonically with increasing temperature, these graphs shows an almost independent of frequency due to their insulating nature at higher temperature [18]. It shows low resistance values in these higher temperature region and the conductivity of the NBMP1 sample is lower than the other samples and NBMP5 showed high resistance values as compared with the other sample due to increasing the Eu^{+3} ion doping concentration [19].

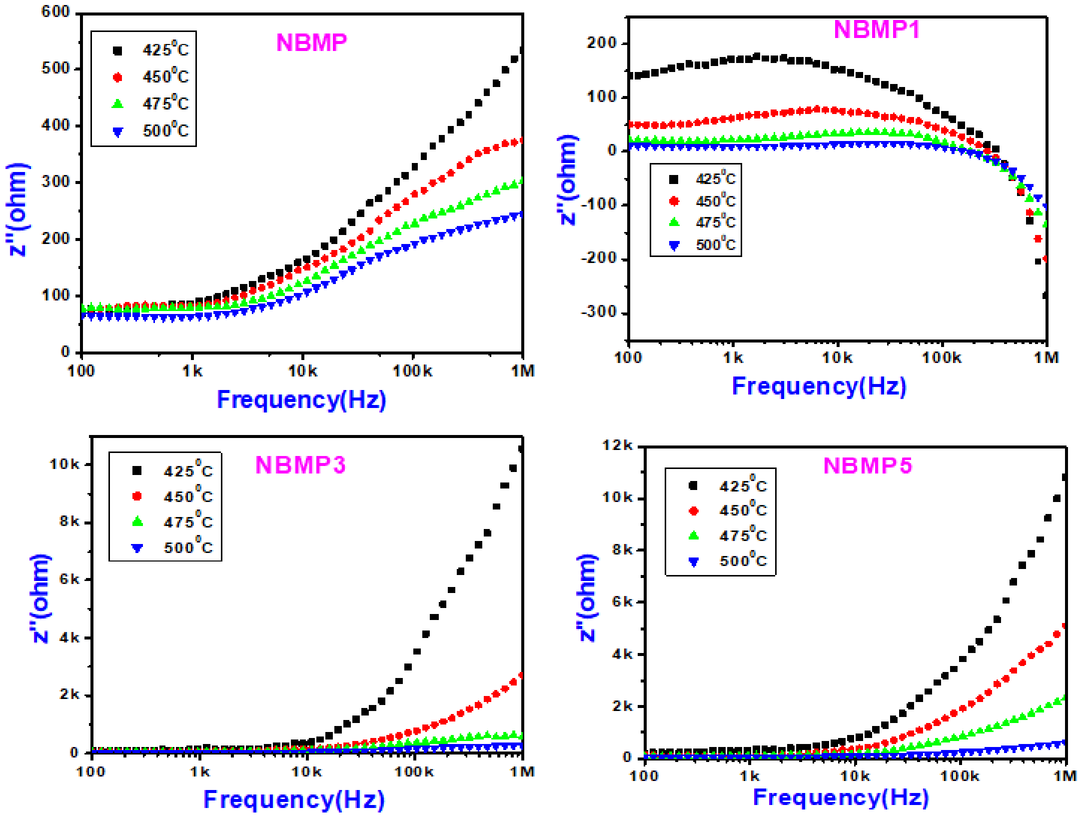

Figure 6: Z'' versus frequency plots of the NBMP, NBMP1, NBMP3 and NBMP5 samples

Figure 6 shows Z" versus frequency at temperatures indicated for $Na_2Ba_{1-x}Eu$ Mg (P_2O_8) compounds. At lower frequencies (Below 10kHz) all the temperature curves are very close to each other (almost merged) and at higher frequencies (above 10kHz) the temperature curves get separated and exhibit tendency of going to a peak. By increasing the temperature imaginary part of impedance (Z") is increasing for all samples. NBMP1 samples showed slightly different behavior [20].

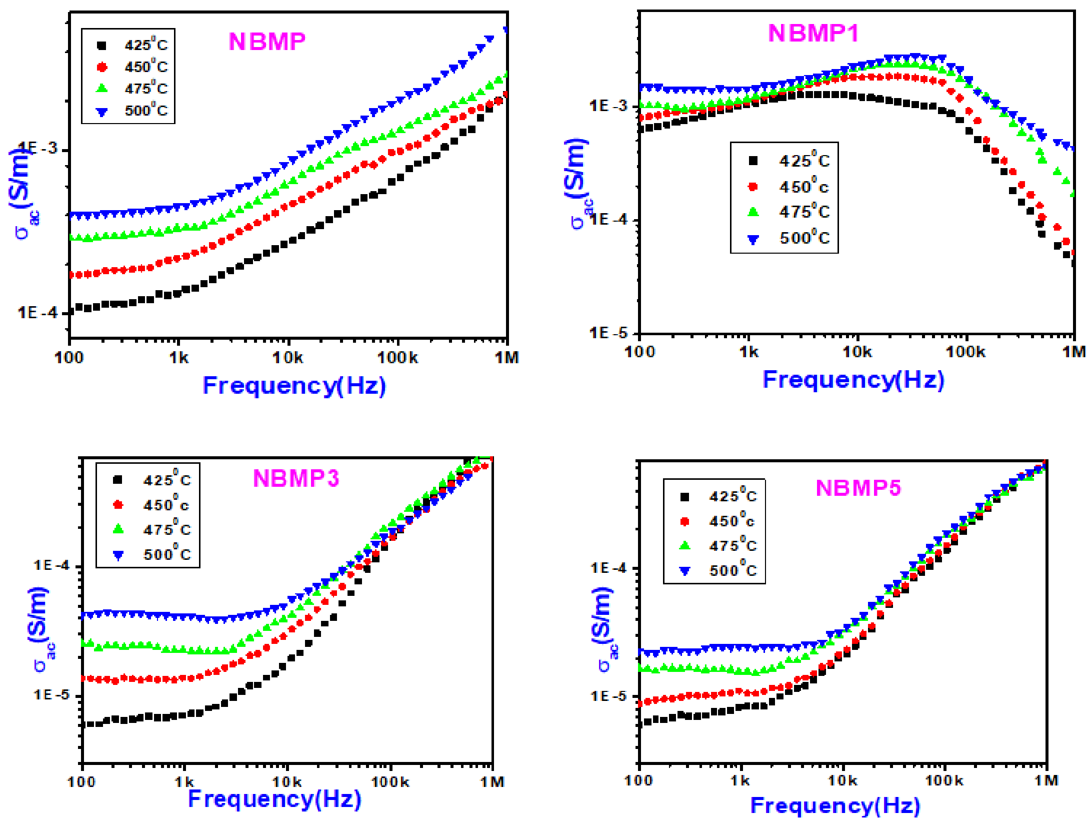

Figure 7: Conductivity variation with frequency of the NBMP, NBMP1, NBMP3 and NBMP5 samples

Conductivity variation of the samples at various temperatures is in figure 7. The AC Conductivity of the system depends on the reactive nature of the sample and the curves show dispersion found for an electrically conducting system. The conductivity curves of all temperatures merge above 100 KHz. At a given temperature, the conductivity decreases with decreasing frequency and its extrapolation gives σdc the conductivity due to the long range translational motion of the charge carriers. The frequency dependent conductivity indicates the presence of space charge polarization in the samples. The activation energies for conductivity are calculated using Arrhenius equation form the plot shown in figure 8 and the values are tabulated in table 4. The activation energies are functions of concentration and frequency. This confirms that the hopping conduction mechanism is dominant in the sample. The DC Conductivity activation energies are also listed in table 4 [21-23].

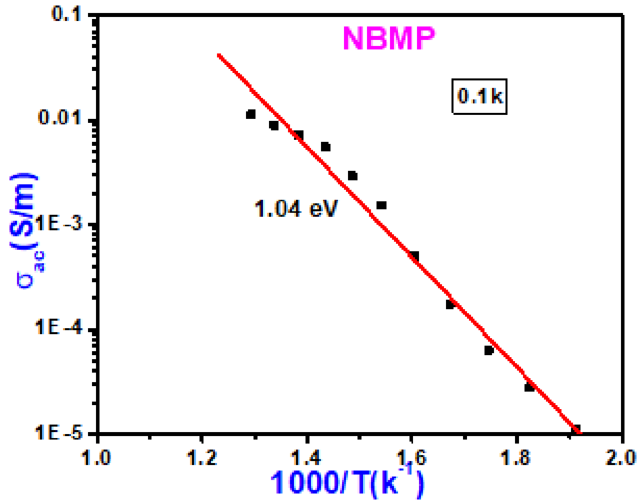

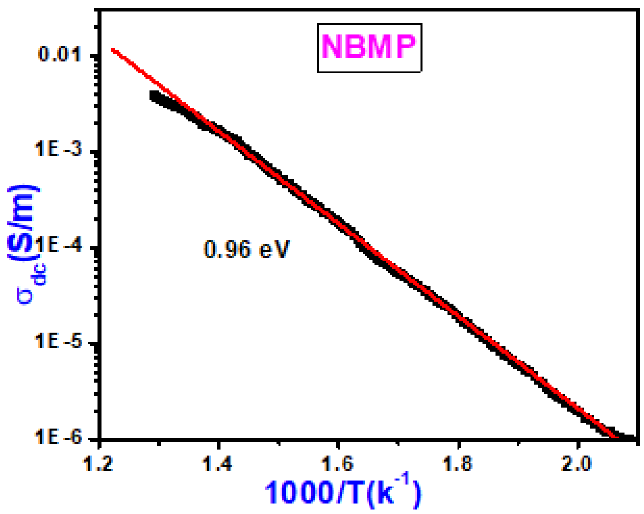

Figure 8: AC and DC conductivity variation with inverse of temperature of the NBMP for sample

Table 4: Activation energies (AC and DC) of the NBMP, NBMP1, NBMP3 and NBMP5 samples

Sample	AC (eV)			DC (eV)
	0.1KHz	0.5KHz	1KHz	
NBMP	1.04	1.03	1.03	0.96
NBMP1	1.23	1.22	1.20	1.30
NBMP3	0.95	0.94	0.92	1.05
NBMP5	0.74	0.54	0.46	1.19

Figure 9 shows the real part of dielectric constant as a function of frequency at different temperature. It is clear from these figures that the dielectric constant is low at high frequency and high at higher temperatures. The larger dielectric constant at higher temperature is due to the orientational polarization which is due to the thermal motion of molecules. "When the temperature is increased the orientation of dipoles is facilitated and this increases the value of orientational polarization, which leads to increase the dielectric constant with temperature" [23-26]. The dielectric behavior of the present samples in the low frequency region is due to orientational polarization and interfacial polarization [27-28].

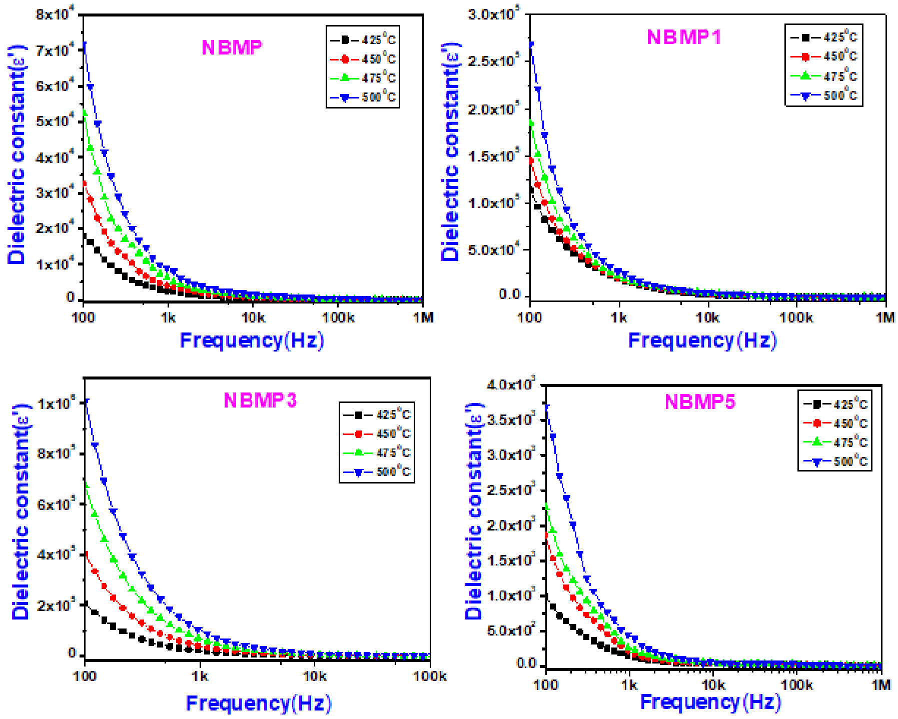

Figure 9: Dielectric Constant (Ɛ') Vs frequency of the NBMP, NBMP1, NBMP3 and NBMP5 samples

Figure 10 shows dielectric loss versus temperatures for all compounds. The dielectric loss is due to the polarization processes which are temperature dependent. Dielectric loss varies linearly with temperature. The dielectric losses are due to various charge transportation mechanisms. The loss due to conduction is due to the migration of ions over large distances. The energy lost per cycle is proportional to σac /ω. The dielectric loss at low frequency is due to various polarization processes that are active. At higher temperatures the conductivity is large due to thermal activation.

The tan δ is high at low frequencies and higher temperatures. This is due to the presence of various polarizations and defects in the samples [29-30]. The presence of associated charges can result in peaks in these curves. The peak s of loss tangent shift with a thermally controlled mechanism. The present samples show the hopping mechanism of electrical conductivity with which thermally activated [31].

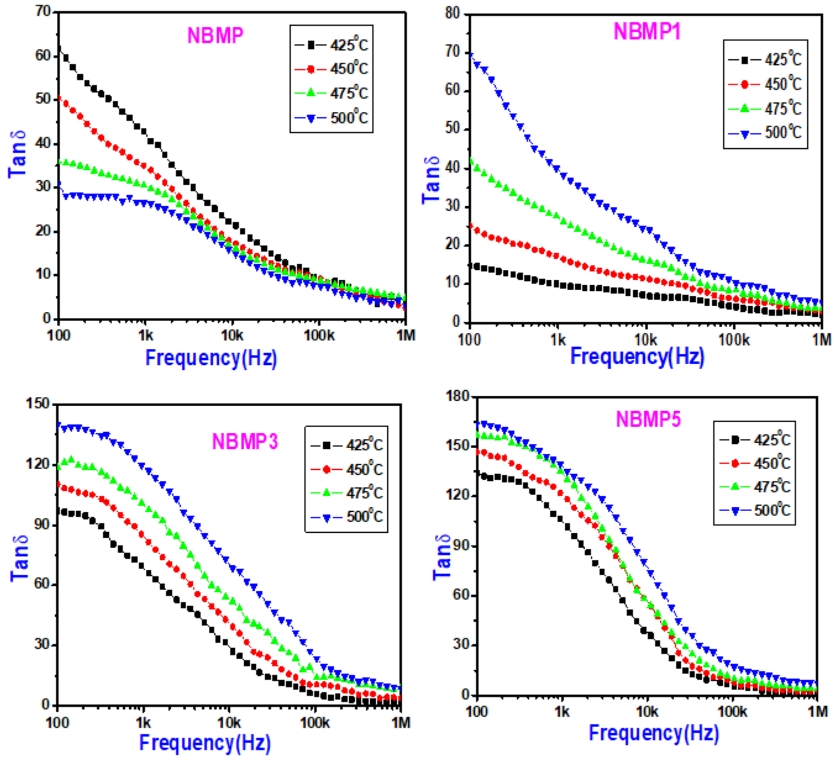

Figure 10: Dielectric loss tangent Vs frequency of the NBMP, NBMP1, NBMP3 and NBMP5 samples

Fig11. (a) Shows the broad bond ranging (200-400nm) with a maximum at 396 nm are charge transfer band (CTB) transition from the 2p orbital of the O^{-2} to the 4f orbital of the Eu^{+3}. The dominant sharp lines in wavelength region of 300-550nm are from the f-f transitions within $4f^9$ configuration of E^{+3} ion. The broad excitation band observed may be attributed to the transition from the fully filled 2p orbital of O^{-2} ions to the partially filled 4f orbital's of Eu^{+3} $_{and}$ may exhibit excitation peaks due to the transitions $7F_0 \rightarrow 5H_6$ at 297nm, $7F_0 \rightarrow 5H_3$ at 318 nm, $7F_0 \rightarrow 5D_4$ at 362 nm, $7F_0 \rightarrow 5L_7$ at 383 nm, $7F_0 \rightarrow 5L_6$ at 396nm respectively. The emission spectrum under the excitation at 396 nm is shown in Fig5. (b). The spectra consist of a number of sharp lines ranging from 400 to 800 nm. Many Emission peaks $5D_0 \rightarrow 7F_1$ at 594 nm, $5D_0 \rightarrow 7F_2$ at 615nm, $5D_0 \rightarrow 7F_3$ at 654 nm, $5D_0 \rightarrow 7F_4$ at 687 nm, $5D_0 \rightarrow 7F_4$ at 699 nm respectively. The intensity of the $5D_0 \rightarrow 7F_1$ is higher than the intensities of the $5D_0 \rightarrow 7F_4$ transition. The PL spectrum Fib5. (b) consist of major line emission at 594nm and minor emission at 654nm, Which can be attributed to the $5D_0 \rightarrow 7F_1$ and $5D_0 \rightarrow 7F_4$ transition of Eu^{+3}, respectively. The emission spectra are dominant by the transition of $5D_0 \rightarrow 7F_1$. The strongest emission peak is located at 594 nm, which indicates that the Eu^{+3} ion occupy inversion symmetry sites in the lattice. According to the Judd-Ofelt theory, the magnetic dipole transition is permitted. The emission spectra are from the different Eu^{+3} concentrations as indicated. Fib11. (b) shows that the intensity increased with concentration from 0.01 to 0.05 mol% of Eu^{+3} and it decreed peak slightly when the concentration was increased. The red emission at 612 nm is an electric dipole transition, while the emission range at 594 nm is a typical magnetic dipole transition. When Eu^{+3} ion is the lattice of inversion symmetry Centre.$5D_0 \rightarrow 7F_1$ magnetic dipole transition Orange-Red light emission will be dominant [1, 12, 33, 34]. Increase in Eu^{+3}doping concentration results in decreasing peak intensity [32].

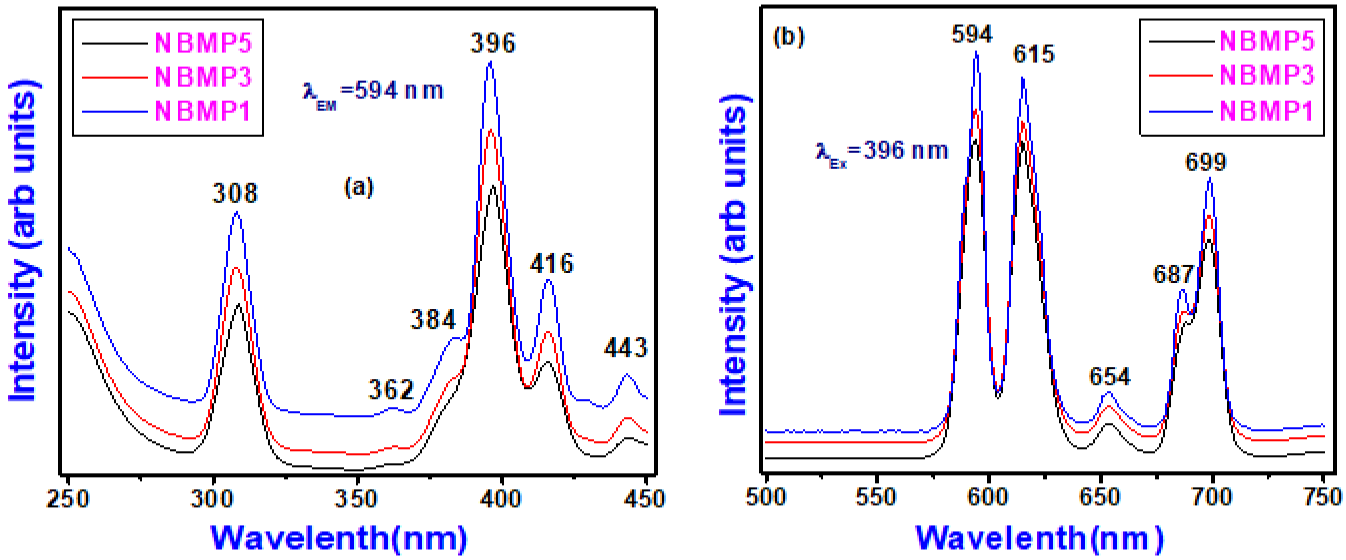

Figure 11: (a) Excitation and (b) Emission spectra of NBMP1, NBMP3 and NBMP5

NBMP1, NBMP3 and NBMP5 samples (0.6080, 0.3898), (0.6272, 0.3702), (0.6239, 0.3718) respectively. The Color coordinates of (X= 0.01, 0.03, 0.05) move to Orange –Red region with varying Eu concentration. The investigate the performance of $Na_2Ba_{1-x}Eu_xMg\ (PO_4)\ _2$ phosphors on colour luminescent emission, the colour coordinates were estimated using CIE 1931 system. Figure 16. shows the chromaticity coordinates calculated. NBMP5 with concentration Eu doped more suitable to emit the red luminescence at 612nm. Favorable for construction red component of WLED's in solid state lighting application. Table 5 color purity is Eu^{+3} doping concentration increase to increased. Additionally color correlated Temperature (CCT) values fall in the range 1700-2000k for different excitation wavelengths [14, 15, 35].

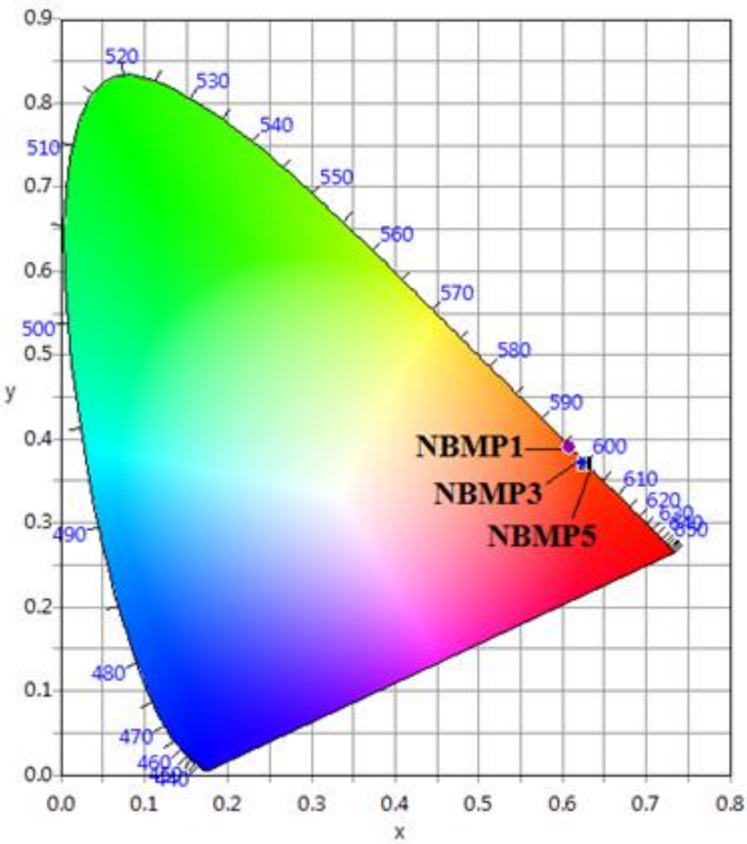

Figure 12: The color spectra chromaticity diagram of NBMP1, NBMP3 and NBMP5 phosphors

Table 5: CIE Chromaticity co-ordinates, color purity and color correlated temperature (CCT) of NBMP1, NBMP3 and NBMP5 samples

Sample	X	Y	Color Purity %	CCT (k)
NBMP1	0.6080	0.3898	83.44	1741
NBMP3	0.6272	0.3702	87.46	1966
NBMP5	0.6239	0.3718	86.65	1926

4. Conclusions

The $Na_2Ba_{1-x}Eu_xMg\ (PO_4)_2$ (where x=0, 0.01, 0.03, and 0.05) are synthesized using solid state sintering method. The samples have rhombohedral structure, with space group: p-3m1 and Lattice parameter varied slightly with the variation of europium concentration. FTIR shows symmetric and symmetric stretch of P-O-P bonds and also bending vibrations. Vibrations corresponding to characteristic peaks of PO_3^{-4} are also observed. The samples show frequency and temperature dependent dielectric properties which vary with composition. Excitation with 256 nm light gives emission peaks due to the transition $5D_0 \rightarrow 7F_1$ at 589 nm, $5D_0 \rightarrow 7F_2$ at 612nm, $5D_0 \rightarrow 7F_3$ at 651 nm, $5D_0 \rightarrow 7F_4$ at 684 nm, $5D_0 \rightarrow 7F_4$ at 696 nm respectively. The samples show orange red emissions.

References

[1] M. Nagpure, K. M. Shinde, Vijay Kumar, O. M. Ntwaeaborwa, S. J. Dhoble, H. C. Swart, Combustion synthesis and luminescence investigation of $Na_3Al_2(PO_4)_3$: RE (RE: ce^{3+}, Eu^{3+} and Mn^{2+}) phosphor, Journal of Alloys and Compounds, 492 (2010) 384-388.

[2] Mao Xia, Xianbo Wu, Yuan Zhong, H. T. (Bert) Hintzen, Zhi Zhou, Jing wang, photoluminescence properties and energy transfer of a novel Sr8ZnY (PO4) 7: Tb^{3+}, Eu^{3+} phosphor with high thermal stability with high potential for application in warm white light emitting diodes, Journal of Material Chemistry C, 00 (2013) 1-3.

[3] Xinyue Li, Xianto Wei, Yanguang Qin, Yonghu Chen, Changkui Duan, Min yin, The emission rise time of Bay2ZnO5: Eu3+ for non – contact luminescence thermometry, Journal of Alloys and Compounds 657 (2016) 353-357.

[4] Peican Chen, Anxiang Guan, Guofang Wang, Siyu Xia, liya Zhou, Ce^{3+} sensisized Na2BaMgP2O8: Mn2+ phosphor: synthesis and photoluminescence properties, J Mater Sci: Mater Electron 27, 6071-6075 (2016).

[5] Amal Boukhris, Benoit Glorieux, Mongi Ben Amara, X-ray diffraction, ^{31}P NMR and europium photoluminescence properties of the $Na_2Ba_{1-x}Sr_xMg\ (PO_4)_2$ system related to the glaserite type structure, Journal of Molecular Structure1083 (2015) 319-329.

[6] Yoshinori Yonesaki, Chihiro Matsuda, Qiang Dong, Structural consideration on the emission properties of Eu2+-doped Li2BaMgP2O8 and orthophosphates, Joournal of Solid State Chemistry 196 (2012) 404-408.

[7] Yoshinori Yonesaki, Sensitized red luminescence from Mn^{2+}-doped Olgite – type phosphates, Journal of Solid State Chemistry 197 (2013) 166-171.

[8] Lu Pan, Xiaozhan yang, chaoyue Xiong, dashen Deng, chunlin Qin and Wenlin Feng, Novel Red –Orange

phosphors $Na_2BaMg(PO_4)_2$: Pr^{3+}: synthesis, Crystal Structure and Photoluminescence Performance, De Gruyter, Z. Naturforsch 2017, 173 (2), 99-103.
[9] Amal Boukhris, Mourad hidouri, Benoit Glorieux, Mongi Ben Amara, $Na_2BaMg(PO_4)_2$: synthesis, crystal structure and europium photoluminescence properties, Journal of Rare Earths, 31, (2013) 849.
[10] Qiguang Xu, Liu Han, Qiumei Di, Jiayue Sun, Tunable Luminescence and efficienent Energy Transfer of $Na_2BaMgP_2O_8$: Eu^{2+}, Tb^{3+} Phosphor for White light-emitting diodes, Ceramics International 41 (2): 2699-2705 (2015).
[11] Tang Wanjun, Fu Tingting, Luminescence and Energy Transfer in Eu^{2+}, Mn^{2+} codoped $Na_2BaMgP_2O_8$, Applied Physics A 114, 931-935 (2014). .
[12] Chao Wei, DenghuinXu, Yetong Jai, Xiong Li, JiayuenSun, Tunable luminescence properties of Ba_2ScTaO_6: $Bi^{3+,}$ Eu^{3+} phosphors, Applied Physics A (2019) 125: 706.
[13] K. Kumar, A. K. Singh, S. B. Rai, Laser excited long lasting luminescence in $CaAl_2O_4$: Eu^{3+}/Eu^{2+} + Nd^{3+} phosphor, Spectrochimica Acta Part A: Molecular and Biomolecular spectroscopy102 (2013) 212-218.
[14] You-Shun Peng, Wei-Wei Sui, Cong-Lin, yan-Yan kang, Yan-su Wang, Zhi-Wei Zhang, Photoluminescence properties of a novel red emitting Ba10F2 (PO4) 6: Eu3+ Phosphor, Spectrochimica Acta Part A: Molecular and Biomolecular Spectroscopy 145 (2015) 194-197.
[15] R. D. Shannon, Revised Effective Ionic redii and Systematic Studies of Internatomic Distances in Halides and halcogenides, Acta Crystal (1976), A32.
[16] Yang Zhang, weitao Gong, jingjie yu, Yuan Lin, Guilling Ning, Tunable white-light emission via energy transfer in single-phase LiGd $(WO^4)_2$: Re^{3+} (Re = Tm, Tb, Dy, Eu) phosphors for UV-excited WLEDs, RSC Advances (2015) 5, 96272-96280.
[17] Yun Zhang, Guangfu Yin, Shisu Zhu, Dali Zhou, Yuehua Wang, Yong Li, Lin Luo, Preparation of b-Ca3 (PO4) 2 bio ceramic powder from calcium carbonate and phosphoric acid, Curent Apllied Physics 5 (2005) 531-534.
[18] Relaxation mechanism of (x) $Mn_{0.45}Ni_{0.05}Zn_{0.50}Fe_2O_4$ + (1 − x) $BaZr_{0.52}Ti_{0.48}O_3$ multiferroic materials, M Azizar Rahman and A K M Akther Hossain, Phys. Scr.89 (2014) 115811 (11pp).
[19] High temperature complex impedance and modulus spectroscopic studies of doped Na0.5-Bi0.5 Tio3-BaTiO3 ferroelectric ceramics, Ch Sameeradevi, M. Buchi Suresh, G. S. kumar and G. Prasad, Ionics (2016) 22: 2363-2377.
[20] Effect of SrTiO3 on dielectric and piezoelectric properties of NBT, A. Rajani Malathi, G. S. Kumar and G. Prasad, Phase Transitions, 2015 Vol.88, No.2, 169-182.
[21] Piezoelectric, impedance, electric modulus and AC conductivity studies on $(Bi_{0.5}Na_{0.5})_{0.95}Ba0_{.05}Tio_3$ ceramics, Ansu K. Royu, Kamal Prasad, Ashutosh Prasad, Processing and Application of Ceramic 7 [2] (2013) 81-91.
[22] Efect of rare earth on dielectric properties of Mn contained unfilled tungsten bronze ceramics, Shan Wu · Chaozhong Sun · Zhe Guo · Changzheng Hu · Laijun Liu · Liang Fang, Journal of Materials Science: Materials in Electronics (2019) 30: 17393–17404.
[23] Electrical and Dielectric Characterization of Na0.5Li0.5Zr2 (Po4) 3, Umaru Ahmadu, Tomas slkus, Abubakar Ohinoyi Musa, Kasim Uthman Isah, Open journal of physical chemistry, 1, 94-103, 2011.
[24] M. Barsoum, Fundamentals of Ceramics, Mc Graw--Hill, New York 1977, p.543.
[25] W. Cao, R. Gerhardt, Solid State Ionics.42, 213 (1990).
[26] T. G. Abdel-Malak, M. E. Kassem, N. S. Aly, S. M. Kalil, Acta Phys. Pol. A 81, 675 (1992).
[27] R. Singh, R. P. Tandon, V. S. Panwar, S. Chandra, J. Appl. Phys.69, 2504 (1991).
[28] Frequency and temperature-dependence of dielectric permittivity and electric modulus studies of the solid solution Ca0.85Er0.1Ti1xCo4x/3O3 (0 # x # 0.1), Ch. Rayssi, S. El. Kossi, J. Dhahri and K. Khirouni, RSC Adv., 2018, 8, 17139-17150.
[29] Frequency and Temperature Dependence of Dielectric Behaviours for Conductive Acrylic Composites, Suat cetiner, Seyma Sirin, Advances in polymer Technology, Vol.35, No.1, 2016.
[30] Temperature and Frequency Dependence of Dielectric Properties of Superconducting Ceramic GdBa2Ca3Cu4O10.5, V. S. Vinila, jayakumari Isac, International Journal of Science and Research, Volume 7, Issue 8, 2018.
[31] Temperature and frequency dependent dielectric response of C3H7NH3PbI3: A new hybrid perovskite, Payal Sengupta, priyabrata Sadhukhan, Apurba Ray, Ruma Ray, Satyaranjan Bhattacharyya and Sachindranath Das, Journal of Applied Physics.127, 204103 (2020).
[32] The luminescence and structural characteristics of Eu^{3+}-doped $NaBaPO_4$ phosphor, Suyin Zhang, Donglei Wei, Rui Zhu, Yanlin huang, Hyo Jin Seo, Ceramics International 37 (2011) 3697-3702.
[33] Novel orange– red emitting phosphor Ba_2ScNbO_6: Eu^{3+} for WLEDs: Synthesis and luminescence properties, Chao Wei, Denghui Xu, Zaifa Yang, Jinling Li, aicong Geng, Xiong Li, Jiayue Sun, Journal of Materials Science: Materials in Electronics (2019) 30, 15512-15520.
[34] photo luminescencent properties of $LiSr_xBa_{1-x}PO_4$: RE^{3+} (RE= Sm^{3+}, Eu^{3+}) f-f transition phosphors, Dong Tu, Yujun Liang, Rong Liu, Zheng cheng, fan yang, Wenlong Yang, Journal of Alloys and Compounds 509 (2011) 5596-5599.
[35] Synthesis and Rational design of Europium and Lanthium Doped Sodium Zinc Mollybdate with Red Emission for Optical Imaging, Nega Jain, Ruchi Paroha, Rajan K. Singh, Siddhartha K. Mishra, Shivendra K. Chaurasiya, R. A. singh and Jai Singh, Scientific reforts (2019) 9: 2472